

You might find this additional information useful...

This article cites 9 articles, 5 of which you can access free at:

<http://ajprenal.physiology.org/cgi/content/full/276/6/F952#BIBL>

This article has been cited by 6 other HighWire hosted articles, the first 5 are:

Parameter estimation for mathematical models of NKCC2 cotransporter isoforms

M. Marcano, H.-M. Yang, A. Nieves-Gonzalez, C. Clausen and L. C. Moore
Am J Physiol Renal Physiol, February 1, 2009; 296 (2): F369-F381.
[\[Abstract\]](#) [\[Full Text\]](#) [\[PDF\]](#)

A mathematical model of rat distal convoluted tubule. I. Cotransporter function in early DCT

A. M. Weinstein
Am J Physiol Renal Physiol, October 1, 2005; 289 (4): F699-F720.
[\[Abstract\]](#) [\[Full Text\]](#) [\[PDF\]](#)

Molecular Physiology and Pathophysiology of Electroneutral Cation-Chloride Cotransporters

G. Gamba
Physiol Rev, April 1, 2005; 85 (2): 423-493.
[\[Abstract\]](#) [\[Full Text\]](#) [\[PDF\]](#)

A numerical model of acid-base transport in rat distal tubule

H. Chang and T. Fujita
Am J Physiol Renal Physiol, August 1, 2001; 281 (2): F222-F243.
[\[Abstract\]](#) [\[Full Text\]](#) [\[PDF\]](#)

Characterization of the thiazide-sensitive Na⁺-Cl⁻ cotransporter: a new model for ions and diuretics interaction

A. Monroy, C. Plata, S. C. Hebert and G. Gamba
Am J Physiol Renal Physiol, July 1, 2000; 279 (1): F161-F169.
[\[Abstract\]](#) [\[Full Text\]](#) [\[PDF\]](#)

Medline items on this article's topics can be found at <http://highwire.stanford.edu/lists/artbytopic.dtl> on the following topics:

Physics .. Kinetic Model
Mathematics .. Linear Equation

Updated information and services including high-resolution figures, can be found at:

<http://ajprenal.physiology.org/cgi/content/full/276/6/F952>

Additional material and information about *AJP - Renal Physiology* can be found at:

<http://www.the-aps.org/publications/ajprenal>

This information is current as of November 27, 2009 .

A kinetic model of the thiazide-sensitive Na-Cl cotransporter

HANGIL CHANG¹ AND TOSHIRO FUJITA²

¹Health Service Center; and ²Fourth Department of Internal Medicine, University of Tokyo, Tokyo 153-8902, Japan

Chang, Hangil, and Toshiro Fujita. A kinetic model of the thiazide-sensitive Na-Cl cotransporter. *Am. J. Physiol.* 276 (*Renal Physiol.* 45): F952–F959, 1999.—The aim of this study was to construct a numerical model of the thiazide-sensitive Na-Cl cotransporter (TSC) that can predict kinetics of thiazide binding and substrate transport of TSC. We hypothesized that the mechanisms underlying these kinetic properties can be approximated by a state diagram in which the transporter has two binding sites, one for sodium and another for chloride and thiazide. On the basis of the state diagram, a system of linear equations that should be satisfied in the steady state was postulated. Numerical solution of these equations yielded model prediction of kinetics of thiazide binding and substrate transport. Rate constants, which determine transitional rates between states, were systematically adjusted to minimize a penalty function that was devised to quantitatively estimate the difference between model predictions and experimental results. With the resultant rate constants, the model could simulate the following experimental results: 1) dissociation constant of thiazide in the absence of sodium and chloride; 2) inhibitory effect of chloride on thiazide binding; 3) stimulatory effect of sodium on thiazide binding; 4) combined effects of sodium and chloride on thiazide binding; 5) dependence of sodium influx on extracellular sodium and chloride; and 6) inhibition of sodium influx by extracellular thiazide. We conclude that known kinetic properties of TSC can be predicted by a model which is based on a state diagram.

sodium-chloride cotransporter; thiazide diuretics; electrolyte metabolism; kinetic model; computer program

THIAZIDE-SENSITIVE Na-Cl cotransporter (TSC) is present in the renal distal tubule where ~10% of filtered sodium and chloride are reabsorbed (6). In the distal tubule, TSC is localized to the luminal cell membrane and contributes to reabsorption of sodium and chloride by facilitating the entry of these ions into the cell. Transport mediated by TSC is blocked by thiazide, and physiological significance of TSC in the maintenance of body sodium balance can be inferred by the efficacy of thiazide in the treatment of human hypertension. Physiological significance of TSC has been further

illustrated recently by the finding that genetic defects in TSC in human subjects caused derangement in electrolyte metabolism (hypokalemia and metabolic alkalosis) known as Gitelman's syndrome (9).

Fanestil and coworkers (1, 13) reported detailed experiments addressing the kinetics of thiazide binding of TSC using renal cortical membranes. They found that 1) metolazone, a diuretic with a thiazide-like mechanism of action, had a high affinity to TSC; 2) chloride inhibited metolazone binding (i.e., the fraction of TSC bound with metolazone); and 3) sodium stimulated metolazone binding. To explain these results, they proposed a conceptual model of TSC, in which there are two binding sites, one that is selective for sodium and another that recognizes chloride and metolazone in a mutually exclusive fashion and in which occupancy of the former site by sodium increases the affinity of the latter site for metolazone.

Success in cDNA cloning of TSC (3, 4) has enabled direct measurement of sodium influx through TSC expressed in *Xenopus laevis* oocytes. Gamba et al. (4) measured sodium influx with various extracellular concentrations of sodium and chloride, and they found that sodium influx was a saturable process and was consistent with a carrier-mediated mechanism cotransporting sodium and chloride with 1:1 stoichiometry. Dependence of sodium influx on extracellular sodium and chloride could be described by Michaelis-Menten equations with Michaelis constants of 25.0 and 13.6 mM, respectively.

Thiazide, when present in the extracellular fluid, inhibits transport by TSC in a dose-dependent manner. The effective concentration of thiazide is significantly higher than the apparent dissociation constant reported in binding studies. For example, hydrochlorothiazide at 100 μ M inhibited sodium influx by 59% (4), whereas the apparent dissociation constant of hydrochlorothiazide is ~100 nM (1). Similar dose dependency of hydrochlorothiazide in inhibiting sodium influx was reported in the urinary bladder of the winter flounder, which is rich in TSC; half-maximal effective concentration was 20–50 μ M (11). Thus effective affinity (10) of thiazide measured by functional studies appears to be 200- to 1,000-fold lower than the apparent affinity measured by binding studies.

The aim of the present study was to develop a numerical model of TSC that predicts quantitatively

The costs of publication of this article were defrayed in part by the payment of page charges. The article must therefore be hereby marked "advertisement" in accordance with 18 U.S.C. Section 1734 solely to indicate this fact.

and coherently these experimental findings. The strategy was 1) to construct a model based on a state diagram, 2) to calculate the predictions of the model by numerically solving the steady-state equations, and 3) to find the set of rate constants with which the model simulates the experimental results best. We have assumed a state diagram that is similar to the one proposed by Fanestil and coworkers, (13) except that in our model thiazide binding can be possible both from the extracellular and intracellular sides. This assumption was considered to be necessary, since our preliminary examination had revealed that a model without intracellular thiazide binding could not simulate the observed discrepancy between effective and apparent affinities of thiazide. Optimal values of rate constants were determined as a minimization problem of a penalty function that was devised to quantitatively estimate the difference between model predictions and experimental results. Systematic search procedure yielded a set of rate constants with which the model could simulate all the experimental results listed above.

METHODS

Experimental data to simulate. We constructed the present model to simulate the published experiments of TSC that addressed kinetics of thiazide binding (1, 13) and substrate transport (4). Specifically, we considered experimental results on kinetics of metolazone binding in the absence of sodium and chloride (1), inhibitory effect of chloride on metolazone binding (see figure 5B in Ref. 13), stimulatory effect of sodium on metolazone binding (see figure 2A in Ref. 13), combined effects of sodium and chloride on metolazone binding (see figure 5A in Ref. 13), dependence of sodium influx on extracellular sodium (see figure 2B in Ref. 4) and chloride (see figure 2C in Ref. 4), and inhibition of sodium influx by extracellular thiazide (4). Values of data points were obtained by tracing the figures in the publications.

State diagram. The state diagram of TSC, which we hypothesized in this study, is illustrated in Fig. 1. TSC molecule ("E") has two binding sites, one for sodium ("Na") and another for chloride ("Cl"). The latter site can also bind thiazide ("D"), but bindings of chloride and thiazide are mutually exclusive. The two sites can be occupied in any order, and occupancy of one site can affect the binding or dissociation processes of the other site. For example, the dissociation rate constant of extracellular sodium when the second site is unoccupied (k_2) can be different from that when the second site is occupied by chloride (k_8). TSC exists either on the extracellular side or on the intracellular side, and states on the intracellular side are indicated by prime mark ('). Only unloaded and fully loaded TSC (E, E', ENaCl, and ENaCl') can cross the cell membrane, and TSC loaded with thiazide cannot cross the membrane.

Steady-state equations. In the steady state, probabilities of finding a TSC molecule in individual states are time-independent and satisfy the system of linear equations (steady-state equations) listed in Table 1. In these equations, the probabilities are represented by bracketed symbols¹ such as [ENa]. Equations M-1 to M-11 indicate that rates of generation and destruction of each state balance each other out. Equation M-12 derives from the definition of these

probabilities and indicates that a TSC molecule should be in one of these states in a given instant. Although similar equations for simpler diagrams with less than six states might be solved manually (8), the steady-state equations for TSC were too complex to be solved in closed form. To circumvent the problem, we developed a computer program that represents and solves the steady-state equations in numerical form. Solution obtained by the program yielded the proportion of TSC bound with metolazone ([ED] + [ENaD] + [ED'] + [ENaD']), and experiments addressing kinetics of metolazone binding could be simulated by altering the concentrations of sodium, chloride, and metolazone. Specifically, experiments examining the effect of chloride on metolazone binding were simulated with [Na] = [Na'] = 0, [Cl] = [Cl'] = 0 ~ 150 mM, and [D] = [D'] = 1 nM. Experiments examining the effect of sodium on metolazone binding were simulated with [Na] = [Na'] = 0 ~ 150 mM, [Cl] = [Cl'] = 0, and [D] = [D'] = 1 nM. Finally, experiments examining metolazone binding in the presence of both sodium and chloride were simulated with [Na] = [Na'] = [Cl] = [Cl'] = 0 ~ 150 mM, and [D] = [D'] = 1 nM. We have made [D] = [D'] in these calculations, because experiments by Fanestil and colleagues (1, 13) were conducted with membrane preparations.

Calculation of unidirectional sodium influx. Unidirectional sodium influx was calculated by extending the original state diagram with radioactive sodium to conform to the actual experimental setup. There were six additional states representing TSC molecule loaded with radioactive sodium (Na*). Specifically, they were ENa*, ENa*D, ENa*Cl, ENa*', ENa*D', and ENa*Cl'. These states were connected to other states similarly as their radioactive counterparts. For example, ENa* was connected with E, ENa*D, and ENa*Cl. Forward and backward rate constants between E and ENa* were k_1 [Na*] and k_2 , respectively. We note that, in this extension of the diagram, no additional rate constants were introduced, since we assumed that bindings and dissociations of radioactive and radioactive sodium were governed by the same set of rate constants. The ratio of [Na*] to [Na] (specific activity in the extracellular space) was set to 0.001 throughout the study. The actual magnitude of this ratio is irrelevant as long as it is sufficiently small. The concentration of

Table 1. A system of equations for the steady state

$(k_1[\text{Na}] + k_3[\text{Cl}] + k_{17} + k_{23}[\text{D}])[\text{E}] - k_2[\text{ENa}] - k_4[\text{ECl}] - k_{18}[\text{E}'] - k_{24}[\text{ED}] = 0$	(M-1)
$(k_2 + k_5[\text{Cl}] + k_{25}[\text{D}])[\text{ENa}] - k_1[\text{Na}][\text{E}] - k_6[\text{ENaCl}] - k_{26}[\text{ENaD}] = 0$	(M-2)
$(k_4 + k_7[\text{Na}])[\text{ECl}] - k_3[\text{Cl}][\text{E}] - k_8[\text{ENaCl}] = 0$	(M-3)
$(k_6 + k_8 + k_{19})[\text{ENaCl}] - k_5[\text{Cl}][\text{ENa}] - k_7[\text{Na}][\text{ECl}] - k_{20}[\text{ENaCl}'] = 0$	(M-4)
$(k_{21}[\text{Na}] + k_{24})[\text{ED}] - k_{22}[\text{ENaD}] - k_{23}[\text{D}][\text{E}] = 0$	(M-5)
$(k_{22} + k_{26})[\text{ENaD}] - k_{21}[\text{Na}][\text{ED}] - k_{25}[\text{D}][\text{ENa}] = 0$	(M-6)
$(k_9[\text{Na}'] + k_{11}[\text{Cl}'] + k_{18} + k_{29}[\text{D}'])[\text{E}'] - k_{10}[\text{ENa}'] - k_{12}[\text{ECl}'] - k_{17}[\text{E}] - k_{30}[\text{ED}'] = 0$	(M-7)
$(k_{10} + k_{13}[\text{Cl}'] + k_{31}[\text{D}'])[\text{ENa}'] - k_9[\text{Na}'][\text{E}'] - k_{14}[\text{ENaCl}'] - k_{32}[\text{ENaD}'] = 0$	(M-8)
$(k_{12} + k_{15}[\text{Na}'])[\text{ECl}'] - k_{11}[\text{Cl}'][\text{E}'] - k_{16}[\text{ENaCl}'] = 0$	(M-9)
$(k_{27}[\text{Na}'] + k_{30})[\text{ED}'] - k_{28}[\text{ENaD}'] - k_{29}[\text{D}'][\text{E}'] = 0$	(M-10)
$(k_{28} + k_{32})[\text{ENaD}'] - k_{27}[\text{Na}'][\text{ED}'] - k_{31}[\text{D}'][\text{ENa}'] = 0$	(M-11)
$[\text{E}] + [\text{ENa}] + [\text{ECl}] + [\text{ENaCl}] + [\text{ED}] + [\text{ENaD}] + [\text{E}'] + [\text{ENa}'] + [\text{ECl}'] + [\text{ENaCl}'] + [\text{ED}'] + [\text{ENaD}'] = 1$	(M-12)

¹ It should be noted that solute concentrations are also indicated by bracketed symbols (for example, [Na], [Cl], and [D] in Eq. M-1).

See METHODS (State diagram) for complete description of variables.

radioactive sodium in the intracellular space was set to zero. Steady-state equations were postulated and solved similarly as in the original state diagram, and unidirectional sodium influx was calculated as $k_{19} [\text{ENa}^*\text{Cl}] - k_{20} [\text{ENa}^*\text{Cl}']$. Experiments examining transport kinetics of TSC could be simulated by altering the concentrations of extracellular sodium and chloride. Specifically, experiments that measured unidirectional sodium influx with various extracellular sodium concentrations were simulated with $[\text{Na}] = 1,000 \times [\text{Na}^*] = 0 \sim 96 \text{ mM}$, $[\text{Cl}] = 96 \text{ mM}$, $[\text{Na}'] = 10 \text{ mM}$, $[\text{Na}^{*'}] = 0$, $[\text{Cl}'] = 40 \text{ mM}$, and $[\text{D}] = [\text{D}'] = 0$. Experiments that measured unidirectional sodium influx with various extracellular chloride concentrations were simulated with $[\text{Na}] = 1,000 \times [\text{Na}^*] = 96 \text{ mM}$, $[\text{Cl}] = 0 \sim 96 \text{ mM}$, $[\text{Na}'] = 10 \text{ mM}$, $[\text{Na}^{*'}] = 0$, $[\text{Cl}'] = 40 \text{ mM}$, and $[\text{D}] = [\text{D}'] = 0$. Unidirectional efflux of sodium and unidirectional influx or efflux of chloride could be calculated similarly by introducing appropriate radioactive substrates.

Parameter search. If we assume the state diagram presented in Fig. 1, then kinetic properties of the model TSC are completely determined by the values of 32 rate constants (k_1 to k_{32}). Ideally these values should be specified on the basis of direct experimental measurements. However, pertinent data about individual rate constants are not available in the case of TSC. Therefore, as an alternative choice, we deduced values of a portion of rate constants from theoretical considerations and indirect experimental data, and we systematically adjusted remaining rate constants to make model predictions as close to experimental results as possible.

Rate constants that are involved in substrate and inhibitor binding ($k_1, k_3, k_5, k_7, k_9, k_{11}, k_{13}, k_{15}, k_{21}, k_{23}, k_{25}, k_{27}, k_{29},$ and k_{31}) were assumed to be diffusion limited (5) and were set to $1.0 \times 10^8 \text{ l} \cdot \text{mol}^{-1} \cdot \text{s}^{-1}$ (2). Value of k_{30} was determined to conform to the apparent dissociation constant of metolazone measured in the absence of sodium and chloride (1). Specifically, the steady-state equations in the absence of substrates become sufficiently simple to be solved in closed form, and the value of k_{30} was determined using the following equation

$$K_D = \frac{k_{17} + k_{18}}{\frac{k_{23}}{k_{24}} \cdot k_{18} + \frac{k_{29}}{k_{30}} \cdot k_{17}} \quad (C-1)$$

where K_D is the apparent dissociation constant of metolazone in the absence of substrates ($4.27 \times 10^{-9} \text{ mol/l}$, Ref. 1). Values of $k_8, k_{16}, k_{20}, k_{22},$ and k_{28} were determined from the following

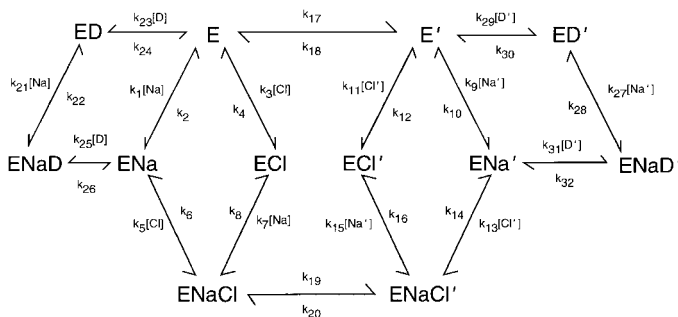


Fig. 1. State diagram for the thiazide-sensitive Na-Cl cotransporter (TSC). Transporter (E) has binding sites for sodium (Na) and chloride (Cl). Thiazide diuretics (D) are assumed to compete for the same binding site with chloride. Sodium and chloride can bind to the transporter in any order. Rate constants of transitional steps are indicated beside arrows. Symbols with brackets, such as "[Na]," stand for concentrations of substrates or thiazide diuretics. Prime mark (') is used to indicate which symbols belong to the intracellular side.

thermodynamic requirements

$$k_1 k_4 k_5 k_8 = k_2 k_3 k_6 k_7 \quad (C-2)$$

$$k_9 k_{12} k_{13} k_{16} = k_{10} k_{11} k_{14} k_{15} \quad (C-3)$$

$$k_1 k_5 k_{10} k_{14} k_{18} k_{19} = k_2 k_6 k_9 k_{13} k_{17} k_{20} \quad (C-4)$$

$$k_1 k_{22} k_{24} k_{25} = k_2 k_{21} k_{23} k_{26} \quad (C-5)$$

$$k_9 k_{28} k_{30} k_{31} = k_{10} k_{27} k_{29} k_{32} \quad (C-6)$$

Values of 12 remaining rate constants ($k_2, k_4, k_6, k_{10}, k_{12}, k_{14}, k_{17}, k_{18}, k_{19}, k_{24}, k_{26},$ and k_{32}) were adjusted to minimize a penalty function that was defined as

$$F = \sum_i \left(\frac{M_i - E_i}{SD_i} \right)^2$$

where M_i are model predictions, E_i are experimental results, and SD_i are standard deviations. Experimental results were comprised of values of data points reproduced in Figs. 2–6 as solid circles (1, 4, 13) and effective affinity of extracellular metolazone in inhibiting substrate transport. The latter value ($4.27 \mu\text{M}$) was deduced from experiments with hydrochlorothiazide (1, 11), since a relevant experiment is not available with metolazone. Standard deviations of experimental results were from representative values found in the original studies (1, 4, 13).

Minimization of the penalty function was conducted using the algorithm of Powell's direction set method (7). This method has the advantage of being applicable to functions whose differentials are difficult to evaluate (as in the present case). It is an iterative method and requires an initial value for each variable to start with. The initial values we used were as follows: $1.0 \times 10^6 \text{ s}^{-1}$ for $k_2, k_4, k_6, k_{10}, k_{12},$ and k_{14} ; $1.0 \times 10^5 \text{ s}^{-1}$ for $k_{17}, k_{18},$ and k_{19} ; $2.0 \times 10^3 \text{ s}^{-1}$ for k_{24} and k_{26} ; and $2.14 \times 10^{-1} \text{ s}^{-1}$ for k_{32} . Thus we started with intrinsic dissociation constants of 10 mM for sodium and chloride on both sides and $2 \mu\text{M}$ for metolazone binding on the extracellular side. Preliminary attempts of minimization revealed that inclusion of $k_{17}, k_{18}, k_{20}, k_{24},$ and k_{26} in optimizing variables resulted in convergence to unrealistic values (including negative values for several rate constants). To circumvent this problem, we imposed the following constraints during the optimization procedure: values of k_{18} and k_{19} should be one of the predefined values ($10^2, 10^3, 10^4, 10^5,$ and 10^6 s^{-1}); and k_{24} should be equal to k_{26} . In the initial step of optimization, an additional constraint was imposed, which preserved the symmetry of intrinsic dissociation constants of sodium and chloride (i.e., $k_2 = k_{10}, k_4 = k_{12},$ and $k_6 = k_{14}$). This constraint, which will be referred to as symmetrical substrate binding hereafter, is a frequently used assumption in modeling transporters, and it simplifies the present model by reducing the number of variables by three. Next, we relaxed the constraint of symmetrical substrate binding and tested whether substantial further reduction in the value of penalty function could be brought about.

Computer hardware and software. The program that solved the steady-state equations and optimized the rate constants was developed for this project using C++ programming language (12). To invert the matrix representing the linear equations, the method of LU decomposition was applied (7). To minimize the penalty function, the function powell in Press et al. (7), which implements the Powell's direction set method in multidimensions, was used after modification for use in C++ language. All the calculations were done in double precision (64-bit IEEE format). The source code was

compiled with Metrowerks C/C++ compiler (version 1.8) running under MacOS. All the development and calculations were conducted with a desktop computer equipped with 180 MHz PowerPC 604e CPU.

RESULTS AND DISCUSSION

The program we developed for this study required 0.2 megabytes of heap memory and less than 0.2 ms to solve the steady-state equations, and it had completed optimization of the rate constants within 3 min. In these calculations most of the computational time was spent in inverting the matrix with LU decomposition. This algorithm is known (7) to require computational time in proportion to the cubic of the dimension of the matrix (i.e., to the cubic of the number of states). Consequently, we speculate that our program would solve the steady-state equations with 17,000 states in less than 10 min. On the other hand, we estimate that the size of heap memory required to store the matrix would become approximately 100 megabytes in the case of a diagram with 3,500 states. Thus, limitation of available computer memory would become a restrictive factor if we apply the program to diagrams with an extremely large number of states. However, for the analysis of most transporters and ionic channels, the present program would be sufficiently fast and compact.

Before optimization of the rate constants, model prediction deviated from the experimental results to a great extent, and the penalty function amounted to 7,943. To improve the model, we first conducted the optimization, which preserved the constraint of symmetrical substrate binding. Despite the constraint, this step of optimization turned out to be highly effective, and the penalty function decreased to as low as 25.813 (a 308-fold reduction). In the actual calculations, values of k_{18} and k_{19} were fixed to one of the predefined values to avoid unrealistic outcome, and the minimal values of the penalty function for all combinations of k_{18} and k_{19} were listed in Table 2. Acceptable outcomes were associated only with restricted combinations of k_{18} and k_{19} , and, among them, the best result was attained when k_{18} and k_{19} were set to 10^5 and 10^3 s⁻¹, respectively. Next, we proceeded with the optimization by removing the

Table 2. Minimized penalty function values with various combinations of k_{18} and k_{19}

k_{19}, s^{-1}	k_{18}, s^{-1}				
	10^6	10^5	10^4	10^3	10^2
10^6	49.6	(1,950)	(107)	(1,570)	(1,600)
10^5	(32.1)	28.5	(2,150)	(131)	(2,630)
10^4	(26.8)	26.6	(2,023)	(2,220)	(2,250)
10^3	26.0	25.8	(35.5)	(1,130)	(1,900)
10^2	79.0	29.8	26.9	132	(1,770)

Penalty function was minimized by systematically adjusting the rate constants while keeping the values of k_{18} and k_{19} to a set of predetermined values. Values of penalty function in parentheses imply that minimization procedure converged to an unrealistic set of rate constants (e.g., negative values for some rate constants). Best result was obtained when k_{18} was 10^5 s⁻¹ and k_{19} was 10^3 s⁻¹.

Table 3. Rate constants

k_1	1.000×10^8	$\text{l} \cdot \text{mol}^{-1} \cdot \text{s}^{-1}$
k_2	4.183×10^5	s^{-1}
k_3	1.000×10^8	$\text{l} \cdot \text{mol}^{-1} \cdot \text{s}^{-1}$
k_4	4.982×10^6	s^{-1}
k_5	1.000×10^8	$\text{l} \cdot \text{mol}^{-1} \cdot \text{s}^{-1}$
k_6	1.065×10^6	s^{-1}
k_7	1.000×10^8	$\text{l} \cdot \text{mol}^{-1} \cdot \text{s}^{-1}$
k_8	8.940×10^4	s^{-1}
k_9	1.000×10^8	$\text{l} \cdot \text{mol}^{-1} \cdot \text{s}^{-1}$
k_{10}	4.183×10^5	s^{-1}
k_{11}	1.000×10^8	$\text{l} \cdot \text{mol}^{-1} \cdot \text{s}^{-1}$
k_{12}	4.982×10^6	s^{-1}
k_{13}	1.000×10^8	$\text{l} \cdot \text{mol}^{-1} \cdot \text{s}^{-1}$
k_{14}	1.065×10^6	s^{-1}
k_{15}	1.000×10^8	$\text{l} \cdot \text{mol}^{-1} \cdot \text{s}^{-1}$
k_{16}	8.940×10^4	s^{-1}
k_{17}	4.587×10^5	s^{-1}
k_{18}	1.000×10^5	s^{-1}
k_{19}	1.000×10^3	s^{-1}
k_{20}	2.180×10^2	s^{-1}
k_{21}	1.000×10^8	$\text{l} \cdot \text{mol}^{-1} \cdot \text{s}^{-1}$
k_{22}	4.183×10^5	s^{-1}
k_{23}	1.000×10^8	$\text{l} \cdot \text{mol}^{-1} \cdot \text{s}^{-1}$
k_{24}	3.192×10^1	s^{-1}
k_{25}	1.000×10^8	$\text{l} \cdot \text{mol}^{-1} \cdot \text{s}^{-1}$
k_{26}	3.192×10^1	s^{-1}
k_{27}	1.000×10^8	$\text{l} \cdot \text{mol}^{-1} \cdot \text{s}^{-1}$
k_{28}	1.389×10^5	s^{-1}
k_{29}	1.000×10^8	$\text{l} \cdot \text{mol}^{-1} \cdot \text{s}^{-1}$
k_{30}	3.514×10^{-1}	s^{-1}
k_{31}	1.000×10^8	$\text{l} \cdot \text{mol}^{-1} \cdot \text{s}^{-1}$
k_{32}	1.166×10^{-1}	s^{-1}

constraint of symmetrical substrate binding. However, it was found that the penalty function decreased only marginally (to 25.801), and we judged it worthless to increase the complexity of the model in terms of the number of independently adjustable rate constants. Thus we adopted the set of rate constants with symmetrical substrate binding. Their values were tabulated in Table 3 and were used in all calculations presented below.

We confirmed that the rate constants in Table 3 indeed satisfy the constraints of Eqs. C-1 to C-6. Furthermore, the constraint of Eq. C-1 predicts that model prediction of the apparent dissociation constant of metolazone in the absence of substrates is identical to the experimental measurement (4.27 nM), and the constraints of Eqs. C-2 to C-6 predict that the net flux becomes zero when $[\text{Na}] \times [\text{Cl}] = [\text{Na}'] \times [\text{Cl}']$. To confirm that these predictions were really fulfilled, we calculated the dissociation constant of metolazone and the net flux in various substrate concentrations and verified that the former was equal to 4.27 nM in all cases and the latter was equal to zero within roundoff errors when $[\text{Na}] \times [\text{Cl}] = [\text{Na}'] \times [\text{Cl}']$.

The result of the simulation that examined the effect of chloride on metolazone binding is presented in Fig. 2. The model predicted a dose-dependent inhibition of metolazone binding by chloride (continuous line), which was in good agreement with experimental results (solid circles). Half-maximal inhibitory concentration of chloride was 61 mM with the model TSC, which was close to the experimental estimate of 60 mM (13). Inhibitory

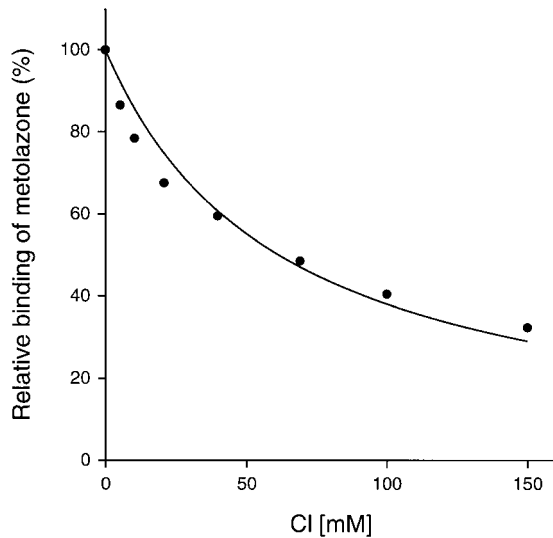


Fig. 2. Inhibitory effect of chloride on metolazone binding. Metolazone binding in various chloride concentrations was examined in absence of sodium. Metolazone was present at 1 nM. Ordinate represents the percent of metolazone bound compared with control, which contained no chloride. Solid circles are experimental results obtained from Tran et al. (see figure 5B in Ref. 13). Solid line shows the model prediction.

effect of chloride on metolazone binding is comprehensible from the structure of the state diagram, in which chloride and metolazone bind competitively and exclusively to the same binding site. We note that, in these experiments and the simulation, concentration of metolazone (1 nM) was much lower than the intrinsic dissociation constant of metolazone on the extracellular side (k_{24}/k_{23} , 319 nM) and binding of metolazone took place mostly on the intracellular side.

The result of the simulation that examined the effect of sodium on metolazone binding is presented in Fig. 3. The model predicted a dose-dependent stimulatory

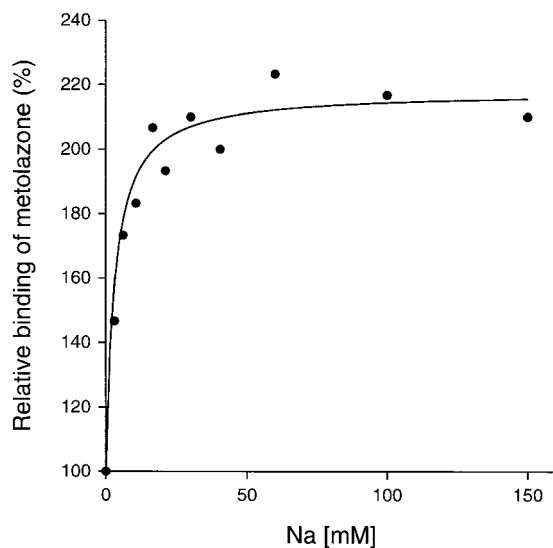


Fig. 3. Stimulatory effect of sodium on metolazone binding. Metolazone binding in various sodium concentrations was examined in absence of chloride. Metolazone was present at 1 nM. Ordinate represents the percent of metolazone bound compared with control, which contained no sodium. Solid circles are experimental results obtained from Tran et al. (see figure 2 in Ref. 13). Solid line shows the model prediction.

effect of sodium on metolazone binding (continuous line), which was in good agreement with experimental results (solid circles). Half-maximal stimulatory concentration of sodium was predicted to be 3.1 mM, which was close to the experimental estimate of 3.7 mM (13). This effect of sodium on metolazone binding could be attributable to the higher affinity of sodium-loaded TSC to metolazone (k_{32}/k_{31} , 1.17 nM) compared with that of unloaded TSC (k_{30}/k_{29} , 3.51 nM) on the intracellular side. Higher sodium concentration promotes transition from unloaded to sodium-loaded TSC and results in higher apparent affinity to metolazone. We note that binding of sodium to TSC on the extracellular side would have an inhibitory effect on metolazone binding due to the low intrinsic affinity to metolazone on this side. However, because of the favorable stability of the model TSC on the intracellular side (see k_{17}/k_{18} and k_{19}/k_{20}), the effect of sodium binding on the intracellular side predominated.

The result of the simulation that examined the combined effects of sodium and chloride on metolazone binding is presented in Fig. 4 (continuous line), which was in agreement with experimental results (solid circles). In this simulation, concentrations of sodium and chloride were changed simultaneously from 0 to 150 mM. At the lower range of concentration, stimulatory effect of sodium prevailed, whereas at the higher range of concentration, inhibitory effect of chloride was predominant. Peak stimulatory effect was observed at 4.4 mM with the model TSC, which was close to the experimental estimate of 4.2 mM (13). Half-maximal inhibitory effect (using the metolazone binding in the absence of sodium and chloride as control) was observed at 62 mM, which was also close to the experimental estimate of 61 mM (13).

Results of the simulations that examined the effects of extracellular sodium and chloride on unidirectional

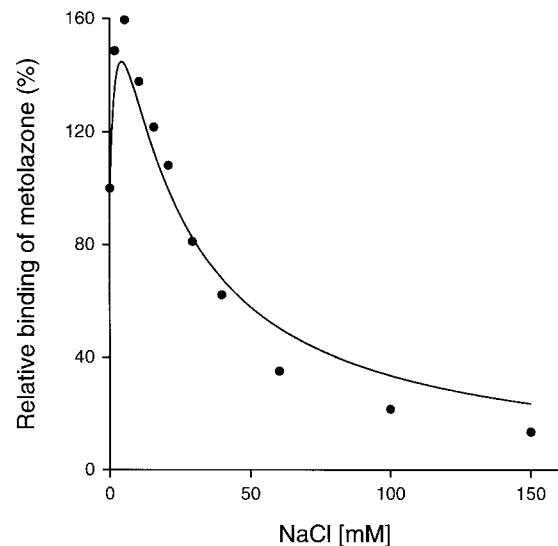


Fig. 4. Combined effects of sodium and chloride on metolazone binding. Metolazone binding was studied in various concentrations of sodium and chloride. Both were present at the same concentrations ranging from 0 to 150 mM. Metolazone was present at 1 nM. Ordinate represents the percent of metolazone bound compared with control, which contained neither sodium or chloride. Solid circles are experimental results reported by Tran et al. (see figure 5A in Ref. 13). Solid line shows the model prediction.

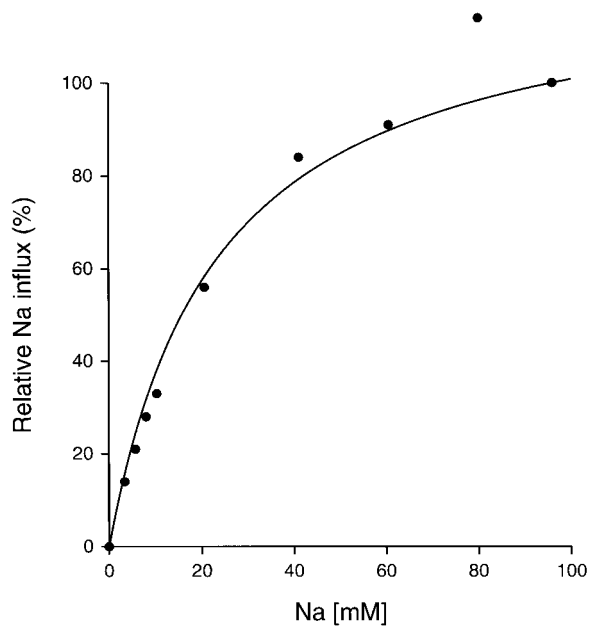


Fig. 5. Dependence of unidirectional sodium influx on extracellular sodium. Unidirectional sodium influx was examined in presence of various concentrations of extracellular sodium. Chloride concentrations in extracellular fluid and intracellular fluid were 96 and 40 mM, respectively. Sodium concentration in intracellular fluid was 10 mM. Metolazone was absent. Sodium influx was normalized by the value observed at 96 mM extracellular sodium. Solid circles are experimental results reported by Gamba et al. (see figure 2B in Ref. 4). Solid line shows the model prediction.

sodium influx are presented in Figs. 5 and 6. Model predictions were plotted in continuous lines, together with experimental results (solid circles) obtained from Gamba et al. (4). Model predictions were in

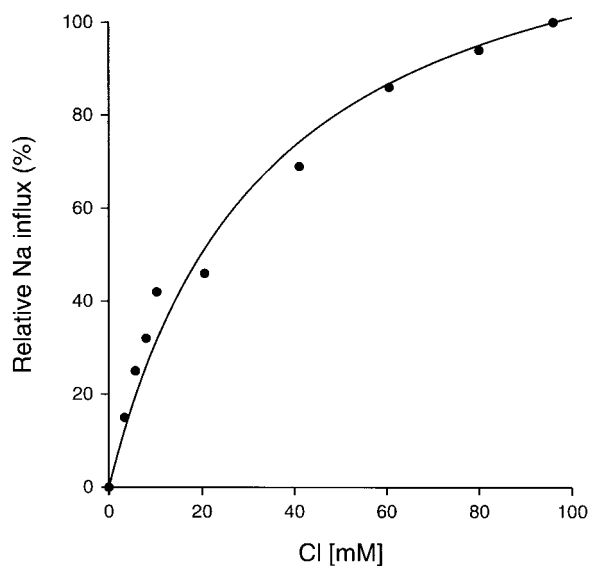


Fig. 6. Dependence of unidirectional sodium influx on extracellular chloride. Unidirectional sodium influx was examined in presence of various concentrations of extracellular chloride. Sodium concentrations in extracellular fluid and intracellular fluid were 96 and 10 mM, respectively. Chloride concentration in intracellular fluid was 40 mM. Metolazone was absent. Sodium influx was normalized by the value observed at 96 mM extracellular chloride. Solid circles are experimental results reported by Gamba et al. (see figure 2C in Ref. 4). Solid line shows the model prediction.

good agreement with experimental results. They reproduced the unidirectional sodium influx as a sodium-dependent (Fig. 5), chloride-dependent (Fig. 6), and saturable process. Half-maximal saturating effects were observed at sodium and chloride concentrations of 29.6 and 31.6 mM, respectively. Whereas the former value was comparable to the Michaelis constant for sodium (25.0 mM) reported by Gamba et al. (4), the latter value was higher than the reported Michaelis constant for chloride (13.6 mM). The cause of the discrepancy is unclear but may be due to the difference in fitting method (nonlinear least square vs. Eadie-Hofstee plot), fitting function (function derived from the steady-state equations vs. function defined by Michaelis-Menten equation), and data to fit to (all data incorporated in the penalty function vs. data plotted in Fig. 6).

To further illustrate the transport kinetics of the model TSC, we plotted transport velocities in both directions as functions of substrate concentrations (Fig. 7). In these calculations, the whence side (e.g., the extracellular side in the case of substrate influx) contained variable concentrations of sodium and chloride, whereas the whither side contained no substrates. When extracellular chloride was fixed to 96 mM, sodium (and chloride) influx was dependent on extracellular sodium (Fig. 7, line A), and half-maximal saturating effect was observed at 3.12 mM. Similarly, sodium efflux was dependent on intracellular sodium (Fig. 7, line B), and half-maximal saturating effect was observed at 1.32 mM. Thus effective affinity for sodium was asymmetric, and was higher on the intracellular side than on the extracellular side. Maximal velocity was also asymmetric, and the maximal influx was 4.54-fold higher than the maximal efflux. Similar properties in transport velocities could be observed when chloride concentrations were varied (Fig. 7, lines C and D). Effective affinity for chloride was 12.9 mM on the extracellular side, and it was 11.1 mM on the intracellular side. Maximal influx was 4.54-fold higher than maximal efflux. These asymmetric transport kinetics in the face of symmetric substrate binding can be ascribed to the different stability of the model TSC across the membrane, and they conform to the theoretical prediction made from analysis of a simple carrier with one substrate and four states (10). The prediction says that if interconversion of loaded transporters is the rate limiting step (which can be seen from Table 3 in the present case), then the side at which the transporter is less stable (extracellular side in the present case) will be the side at which transport will half-saturate at higher concentration and from which the maximal velocity of transport will be greater.²

² In his original report, Stein (10) actually did an analysis of the case in which interconversion of unloaded transporters was the rate limiting step, and he predicted higher effective affinity and lower maximal velocity on the less stable side. However, equation 1 in his report (10), from which the prediction originates, is valid irrespective of which step is the rate limiting step, and we can derive, based on the same equation, the predictions appropriate when interconversion of loaded transporters is the rate-limiting step.

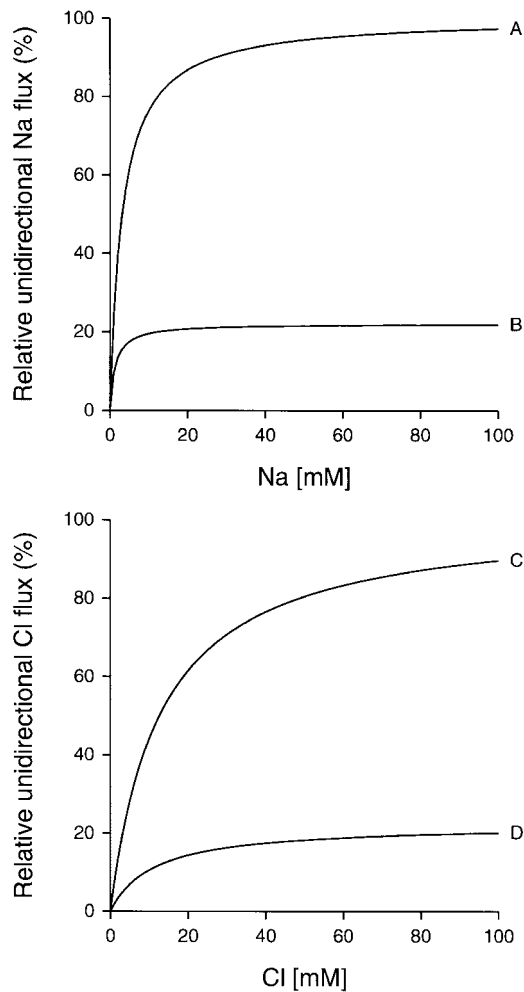


Fig. 7. Asymmetry of transport kinetics of the model TSC. *Top*: transport velocities as functions of sodium concentrations. *Line A*: unidirectional sodium influx with various extracellular sodium concentrations. Extracellular chloride concentration was 96 mM. Both sodium and chloride were absent from intracellular side. *Line B*: unidirectional sodium efflux with various intracellular sodium concentrations. Intracellular chloride concentration was 96 mM. Both sodium and chloride were absent from extracellular side. Transport velocities were normalized by the maximal velocity of sodium influx. *Bottom*: transport velocities as functions of chloride concentrations. *Line C*: unidirectional chloride influx with various extracellular chloride concentrations. Extracellular sodium concentration was 96 mM. Both sodium and chloride were absent from intracellular side. *Line D*: unidirectional chloride efflux with various intracellular chloride concentrations. Intracellular sodium concentration was 96 mM. Both sodium and chloride were absent from extracellular side. Transport velocities were normalized by the maximal velocity of chloride influx.

Model prediction of half-maximal effective concentration of metolazone to inhibit sodium influx was 4.27 μM , which was identical to the experimental value we used to calculate the penalty function. This value was 1,000-fold higher than the apparent dissociation constant for metolazone in the absence of substrates. One of the causes of this difference would be the asymmetry of intrinsic dissociation constant for metolazone: 0.32 μM on the extracellular side vs. 3.51 nM (k_{30}/k_{29}) on the intracellular side. In the case of the experiments and simulations studying effective affinity to metolazone,

metolazone is present only on the extracellular side and cannot bind to the high-affinity binding site present on the intracellular side.

In conclusion, a model of TSC that was based on a state diagram with one cation-binding site and one anion-binding site can reproduce the known kinetics of inhibitor binding and substrate transport of TSC. This model is useful in summarizing the experimental data, as well as in predicting transport velocities in various physiological conditions. The computer program we developed is estimated to be sufficiently general and efficient to be applied to transporters and ionic channels involved in renal epithelial transport.

APPENDIX

Solution of the Steady-State Equations in a Closed Form

Inspection of Table 3 reveals that magnitudes of rate constants involved in interconversions of unloaded and fully loaded transporters (k_{17} , k_{18} , k_{19} , and k_{20}) are smaller than most of the rate constants involved in substrate binding and dissociation. This finding suggests that the steady-state equations may be simplified on the basis of rapid equilibrium, which implies that all the processes of binding and dissociation are in equilibrium on both sides of the membrane. The simplified steady state equations can be solved in a closed form as follows³

$$[E] = \frac{N}{D}$$

$$[E\text{Na}] = \frac{\alpha N}{D}$$

$$[E\text{Cl}] = \frac{\beta N}{D}$$

$$[E\text{NaCl}] = \frac{\gamma N}{D}$$

$$[E'] = \frac{N'}{D}$$

$$[E\text{Na}'] = \frac{\alpha' N'}{D}$$

$$[E\text{Cl}'] = \frac{\beta' N'}{D}$$

$$[E\text{NaCl}'] = \frac{\gamma' N'}{D}$$

where

$$\alpha = \frac{k_1}{k_2} [\text{Na}]$$

$$\beta = \frac{k_3}{k_4} [\text{Cl}]$$

³ In these calculations, states bound with thiazide were neglected. However, extending the formula by taking these states into account is straightforward.

$$\gamma = \frac{k_1 k_5}{k_2 k_6} [\text{Na}][\text{Cl}]$$

$$\alpha' = \frac{k_9}{k_{10}} [\text{Na}']$$

$$\beta' = \frac{k_{11}}{k_{12}} [\text{Cl}']$$

$$\gamma' = \frac{k_9 k_{13}}{k_{10} k_{14}} [\text{Na}'][\text{Cl}']$$

$$N = k_{18} + k_{20}\gamma'$$

$$N' = k_{17} + k_{19}\gamma$$

and

$$D = N(1 + \alpha + \beta + \gamma) + N'(1 + \alpha' + \beta' + \gamma')$$

When substrate concentrations are sufficiently high, these formulas provided a good approximation. For example, if we assume $[\text{Na}] = [\text{Cl}] = 40$ mM, $[\text{Na}'] = 10$ mM, and $[\text{Cl}'] = 40$ mM, then values calculated with these formulas were identical to the true values with less than 1% of relative error. However, as substrate concentrations on either side of the membrane decrease, binding processes of substrates become slower and the assumption of rapid equilibrium becomes less appropriate. For example, if we assume $[\text{Na}] = [\text{Cl}] = 1$ mM, $[\text{Na}'] = 10$ mM, and $[\text{Cl}'] = 40$ mM, then relative error of $[\text{ENaCl}]$ calculated with the formula is as high as 29.2%. Thus, although the formulas derived from the assumption of rapid equilibrium may be accurate at the physiological range of substrate concentrations, they should be used with caution when substrate concentrations are low on either side of the membrane.

Address for reprint requests and other correspondence: H. Chang, Health Service Center, Univ. of Tokyo, 3-8-1 Komaba, Meguro-ku, Tokyo 153-8902, Japan.

Received 27 April 1998; accepted in final form 20 January 1999.

REFERENCES

1. **Beaumont, K., D. A. Vaughn, and D. D. Fanestil.** Thiazide diuretic drug receptors in rat kidney: identification with [³H]metolazone. *Proc. Natl. Acad. Sci. USA* 85: 2311–2314, 1988.
2. **Benjamin, B. A., and E. A. Johnson.** A quantitative description of the Na-K-2Cl cotransporter and its conformity to experimental data. *Am. J. Physiol.* 273 (*Renal Physiol.* 42): F473–F482, 1997.
3. **Chang, H., K. Tashiro, M. Hirai, K. Ikeda, K. Kurokawa, and T. Fujita.** Identification of a cDNA encoding a thiazide-sensitive sodium-chloride cotransporter from the human and its mRNA expression in various tissues. *Biochem. Biophys. Res. Commun.* 223: 324–328, 1996.
4. **Gamba, G., S. N. Saltzberg, M. Lombardi, A. Miyanoshita, J. Lytton, M. A. Hediger, B. M. Brenner, and S. C. Hebert.** Primary structure and functional expression of a cDNA encoding the thiazide-sensitive, electroneutral sodium-chloride cotransporter. *Proc. Natl. Acad. Sci. USA* 90: 2749–2753, 1993.
5. **Hille, B.** *Ionic Channels of Excitable Membranes* (2nd ed.). Sunderland, MA: Sinauer, 1992.
6. **Malnic, G., R. M. Klose, and G. Giebisch.** Micropuncture study of distal tubular potassium and sodium transport in rat nephron. *Am. J. Physiol.* 211: 529–547, 1966.
7. **Press, W. H., B. P. Flannery, S. A. Teukolsky, and W. T. Vetterling.** *Numerical Recipes in C*. Cambridge, NY: Cambridge University Press, 1988.
8. **Sanders, D., U.-P. Hansen, D. Gradmann, and C. L. Slayman.** Generalized kinetic analysis of ion-driven cotransport systems: a unified interpretation of selective ionic effects on Michaelis parameters. *J. Membr. Biol.* 77: 123–152, 1984.
9. **Simon, D. B., C. Nelson-Williams, M. J. Bia, D. Ellison, F. E. Karet, A. M. Molina, I. Vaara, F. Iwata, H. M. Cushner, M. Koolen, F. J. Gainza, H. J. Gitelman, and R. P. Lifton.** Gitelman's variant of Bartter's syndrome, inherited hypokalaemic alkalosis, is caused by mutations in the thiazide-sensitive Na-Cl cotransporter. *Nature Genet.* 12: 24–30, 1996.
10. **Stein, W. D.** Intrinsic, apparent, and effective affinities of co- and countertransport systems. *Am. J. Physiol.* 250 (*Cell Physiol.* 19): C523–C533, 1986.
11. **Stokes, J. B.** Sodium chloride absorption by the urinary bladder of the winter flounder. *J. Clin. Invest.* 74: 7–16, 1984.
12. **B. Stroustrup.** *The C++ Programming Language* (3rd ed.). Reading, MA: Addison-Wesley, 1997.
13. **Tran, J. M., M. A. Farrell, and D. D. Fanestil.** Effect of ions on binding of the thiazide-type diuretic metolazone to kidney membrane. *Am. J. Physiol.* 258 (*Renal Fluid Electrolyte Physiol.* 27): F908–F915, 1990.